INORGANIC CHEMISTRY FRONTIERS

RESEARCH ARTICLE

View Article Online
View Journal | View Issue

Cite this: *Inorg. Chem. Front.*, 2023, **10**, 675

Atomically dispersed copper catalysts for highly selective CO_2 reduction†

Ruirui Yun, *[a] Beibei Zhang,[a] Changsong Shi,[a] Ruiming Xu,[a] Junjie Mao*[a] and Zhaoxu Wang*[b]

Received 27th October 2022,
Accepted 27th November 2022

DOI: 10.1039/d2qi02288e

rsc.li/frontiers-inorganic

Support substrates play important roles in the catalysis process. Herein, atomically dispersed CuN_3 catalysts supported by two different types of zirconia (denoted as CuN_3/NC/T-ZrO_2 and CuN_3/NC/M-ZrO_2) have been rationally fabricated to uncover the influence of the support. CuN_3/NC/T-ZrO_2 exhibits outstanding performance for electrochemical CO_2 reduction towards CO at a wide range of potentials (~96%, 0.6–0.8 V *vs.* RHE) owing to the acidic uncoordinated Zr^{4+} sites of T-ZrO_2, which facilitate CO_2 accumulation, and N-doped carbon (NC), which enhances the conductivity of the catalyst. Moreover, density functional theory calculations prove that T-ZrO_2 effectively decreases the Gibbs free energy for CO_2 to CO conversion. Significantly, this study reports the effects of the substrate on the electrocatalytic CO_2RR and provides a promising strategy for tuning catalytic activity and selectivity during the process of converting CO_2 into high-value products by controlling the phase of the support for the first time.

Introduction

As the consumption of fossil fuels increases, climate change has become a major global issue owing to sea-level rise and global warming.[1] In recent years, many efforts have been made to convert CO_2 into useful chemical feedstocks by designing and tuning appropriate catalytic active sites.[2] These strategies are key to reducing fossil fuel dependence. Among them, the electrochemical CO_2 reduction reaction (EC-CO_2RR) has been considered a promising route to obtain value-added products such as methane, formate, and CO.[3] However, the major competitive process of the H_2 evolution reaction (HER) during the EC-CO_2RR must be suppressed.[4] Hence, it is necessary to develop robust electrocatalysts to selectively produce target products during the EC-CO_2RR process.[5]

Atomically dispersed single metal site catalysts are a new research topic that has attracted increasing attention. These catalysts are a promising technology with tunable active sites and substrates, aiming at higher activity and selectivity during heterogeneous catalytic reactions.[6] Additionally, Cu species, as an abundant non-noble metal, have excellent performance in catalytic systems. Some examples include electrochemical CO_2 reduction by Cu-based MOFs and Cu particles,[7] Cu clusters for CO_2 methanation,[8] and single Cu atoms applied to the O_2 evolution reaction.[9] Additionally, the interaction between the catalyst and support is an important factor in the activity of catalysts.[10] Zirconia is a commonly used substrate with many advantages, such as high thermal stability, good mechanical performance, and the presence of various phases with different chemical and physical characteristics.[11] Some of the most widely used Cu/ZrO_2 catalysts for the conversion of CO_2 include Cu and Cu oxides combined with zirconia present in monoclinic or tetragonal phases.[12]

To explore the influence of different substrates on catalytic performance, we designed two catalysts with atomically dispersed CuN_3 sites supported on zirconia with monoclinic (CuN_3/NC/M-ZrO_2) and tetragonal (CuN_3/NC/T-ZrO_2) phases. The synthetic approach has been simply divided into three steps, as illustrated in Scheme 1. There are equal Lewis and Brønsted acid centers in M-ZrO_2, and water is a Lewis base that can be concentrated by M-ZrO_2, while only the Brønsted acid sites of T-ZrO_2 suppress the HER during the EC-CO_2RR. As expected, the atomically dispersed CuN_3 sites favoured the reduction of CO_2, while the formation of strong metal–support interactions contributed to the enrichment of different reactants, resulting in the diverse catalytic activity of catalysts for the EC-CO_2RR. CuN_3/NC/T-ZrO_2 exhibits high activity for the EC-CO_2RR to produce CO with high faradaic efficiency of up to 96%, while CuN_3/NC/M-ZrO_2 exhibits negligible CO_2RR activity with H_2 as the main product.

[a]*The Key Laboratory of Functional Molecular Solids, Ministry of Education, College of Chemistry and Materials Science, Anhui Normal University, Wuhu 241000, China. E-mail: ruirui58@ahnu.edu.cn, maochem@ahnu.edu.cn*
[b]*Key Laboratory of Theoretical Chemistry and Molecular Simulation of Ministry of Education, School of Chemistry and Chemical Engineering, Hunan University of Science and Technology, Xiangtan 411201, China. E-mail: hnust_chem@163.com*
† Electronic supplementary information (ESI) available. See DOI: https://doi.org/10.1039/d2qi02288e

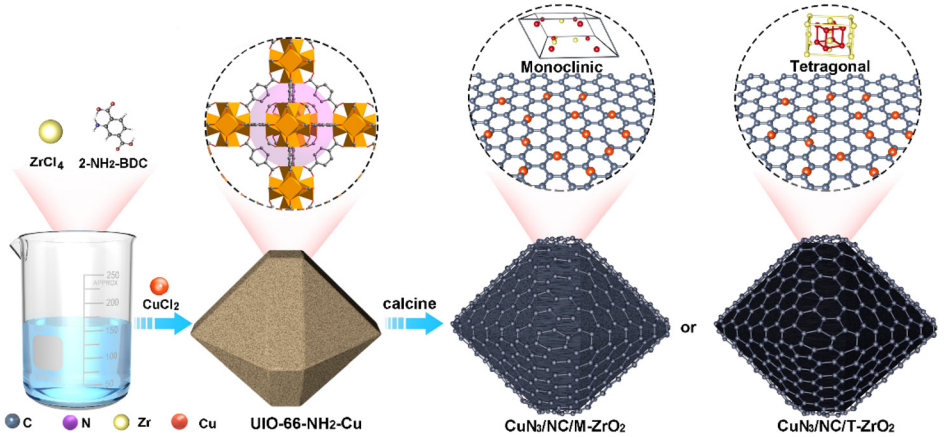

Scheme 1 Schematic illustration of the synthesis of atomically dispersed Cu sites supported on zirconia.

Results and discussion

Singly dispersed CuN_3 sites were formed by pyrolyzing UIO-66-NH_2-Cu, which prevents metal from aggregating owing to coordination bonds between the Cu and $-NH_2$ groups (ESI, Fig. S1†). The powder X-ray diffraction (PXRD) patterns of CuN_3/NC/T-ZrO_2, CuN_3/NC/M-ZrO_2, and CuN_3/NC possess a broad peak around 26° assigned to the (002) peaks of defective graphitic stacking, which allows the Cu atom to be isolated on the substrate support. The absence of significant Cu peaks in the PXRD profiles also agrees with the structural interpretation (Fig. S2†). The N_2 and CO_2 adsorption isotherms reveal that CuN_3/NC/T-ZrO_2 exhibits better BET surface area and CO_2 uptake than CuN_3/NC/M-ZrO_2, indicating that CuN_3/NC/T-ZrO_2 possesses high CO_2 affinity that facilitates CO_2 conversion (Fig. S4 and S5†). Scanning electron microscopy (SEM) and transmission electron microscopy (TEM) images show no clear evidence of particles (Fig. 1b–d). However, high-resolution scanning transmission electron microscopy (STEM) does not exhibit particles, indicating atomically dispersed Cu sites in the structure (Fig. 1f). As is well known, singly dispersed metal sites cannot exist solely on zirconia or carbon support owing to their higher surface energy. Hence, the N-doped carbon matrix obtained *via* the pyrolysis of UIO-66-NH_2 plays an efficient role in fixing singly dispersed Cu sites through the formation of Cu–N bonds. As elemental mapping analysis shows, the homogeneous distribution of Cu, N, C, Zr, and O verifies that the Cu sites are dispersed uniformly over the substrate (Fig. 1g).

Thereafter, X-ray photoelectron spectroscopy (XPS) was performed to verify the chemical formation of CuN_3/NC/T-ZrO_2. The XPS spectra confirm the existence of Cu, Zr, N, O, and C. The N 1s spectrum of the catalyst exhibits three deconvoluted peaks of 398.0 eV (pyridinic-N), 399.4 eV (Cu–N), and 400.3 eV (graphitic-N). This N distribution corresponds to previous reports on singly dispersed metal site catalysts, and the pyridinic-N forms a Cu–N bond. The two main peaks in the O 1s spectrum at 529.9 and 531.3 eV are attributed to the contribution of O bonded to Zr, which is consistent with the Zr 3d spectrum (Fig. 2c). The full width at half maximum of the peak in the Zr 3d spectra is approximately 1.5 eV, which verifies the existence of the tetragonal phase in the sample. The Zr $3d_{5/2}$ peak is located at 181.8 eV with a deviated value of 2.4 eV, which indicates the full oxidation of Zr^{4+} in accordance with the PXRD results. Furthermore, there is no evidence of Cu nanoparticles or clusters from the Zr 3d and O 1s spectra. The Cu $2p_{3/2}$ spectrum at 933.0 eV with a spread shape and spin–obit deviation of 19.0 eV indicates that Cu largely differs from the metallic form and oxidation state.[13]

X-ray absorption near-edge structure (XANES) and extended X-ray absorption fine structure (EXAFS) were further employed to investigate the local atomic structure of CuN_3/NC/T-ZrO_2. As shown in Fig. 2e, the absorption edge of CuN_3/NC/T-ZrO_2 was located between that of Cu foil and CuO, indicating that the atomically dispersed Cu atoms are positively charged in CuN_3/NC/T-ZrO_2. This result coincided with the aforementioned XPS results. Fig. 2f shows the Fourier transform (FT) k^3-weighted extended EXAFS spectrum of CuN_3/NC/T-ZrO_2. Only one dominant peak is observed at about 1.5 Å, which is attributed to the Cu–N first coordination shell. No apparent Cu–Cu coordination peaks in the FT-EXAFS spectrum of CuN_3/NC/T-ZrO_2 are observed, demonstrating that the Cu atoms are atomically dispersed in the support. The quantitative structural parameters of Cu in CuN_3/NC/T-ZrO_2 were obtained by EXAFS fitting, and the fitting curves are shown in Fig. 2g and h. The fitting results indicate that the coordination number of Cu is about 3 (Cu–N_3), and the corresponding Cu–N mean bond length is 1.95 Å. The optimized atomic structure model of the sample is shown in Fig. 2h.

The electrochemical activity towards the CO_2RR of the as-synthesized catalysts was evaluated in a three-electrode system in a high-purity CO_2-saturated 0.5 M $KHCO_3$ (pH 6.8) aqueous solution. The obtained gaseous products (CO and H_2) were monitored using gas chromatography (GC), and no liquid products were detected using ^{1}H nuclear magnetic resonance (NMR) spectroscopy (Fig. S6†). As revealed using linear sweep

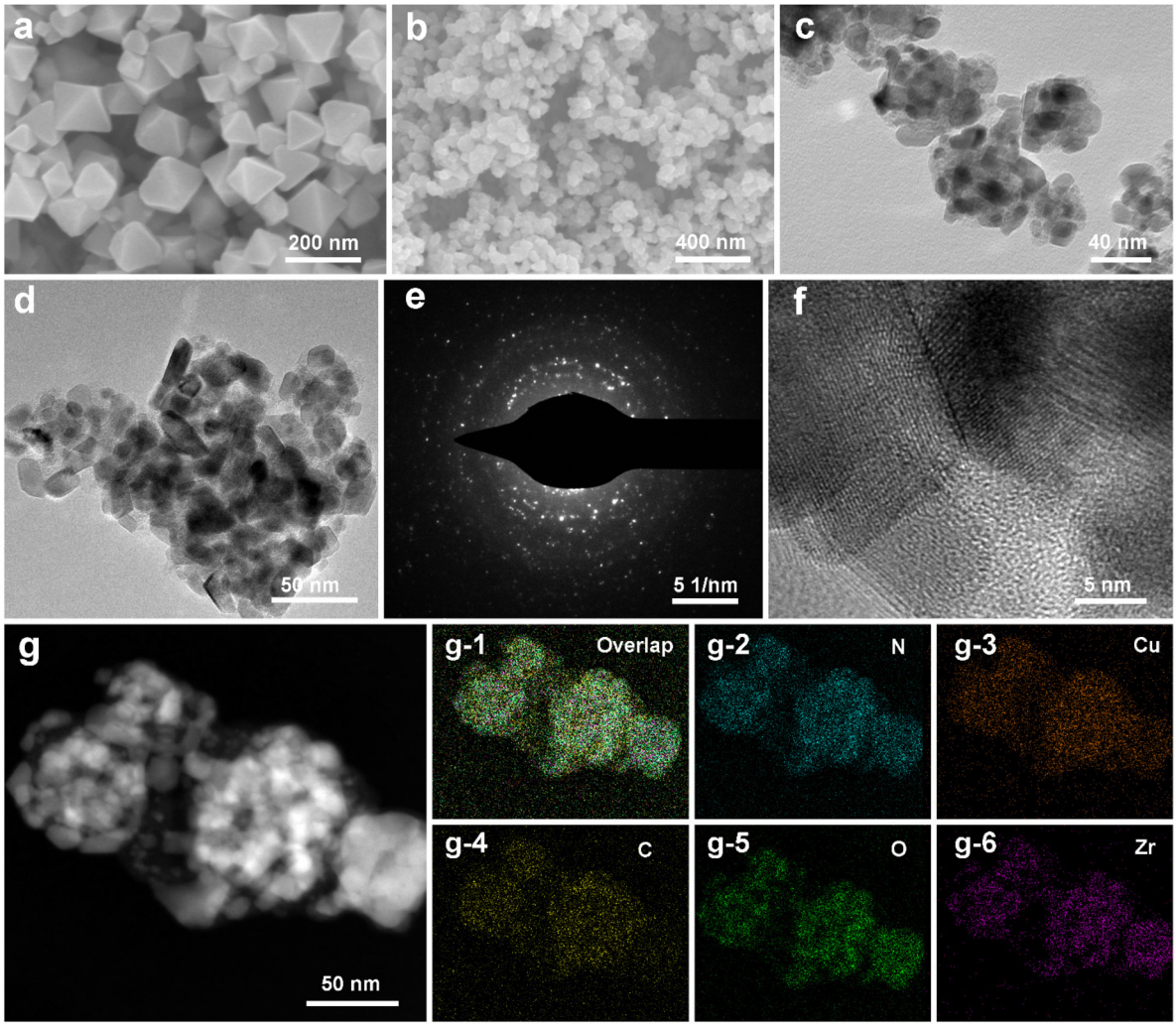

Fig. 1 (a) SEM image of Cu-UIO-66-NH_2. (b and c) SEM and TEM images of CuN_3/NC/T-ZrO_2. (d–f) TEM, selected area electron diffraction (SAED), and STEM images of CuN_3/NC/T-ZrO_2. (g) EDS elemental mapping of CuN_3/NC/T-ZrO_2.

voltammetry (Fig. 3a), CuN_3/NC/T-ZrO_2 and CuN_3/NC/M-ZrO_2 exhibit lower total current density than CuN_3/NC as ZrO_2 is an insulator. However, CuN_3/NC/T-ZrO_2 exhibits larger current densities of 5 mA cm^{-2} at −0.7 V and 12 mA cm^{-2} at −1.0 V (*vs.* RHE, Fig. 3a), indicating the importance of the N-doped carbon substrate towards facilitating electron transfer. Interestingly, the catalytic conversion of CO_2 to CO is considerably affected by the phase of the ZrO_2 substrate. In the case of T-ZrO_2, the FE_{CO} is almost 94% (higher than other Cu-based catalysts, Table S2†) at wide potential ranges of −0.6 V_{RHE} to 0.8 V_{RHE}, while M-ZrO_2 shows no activity for the CO_2RR and is more selective to the HER through the entire potential range. In contrast, when zirconia was etched by hydrofluoric acid, the catalyst retained moderate activity towards CO_2 to CO and with increasing overpotential, the HER is enhanced (Fig. 3b). The higher CO_2 to CO activity indicates the key role of the tetragonal ZrO_2 phase substrate. Compared with T-ZrO_2, in the M-ZrO_2 phase, acidic uncoordinated Zr^{4+} sites change to basic uncoordinated O^{2-} sites, which reject the C═O bond to reduce the collision between C═O and the catalyst and decrease CO_2 activity. Additionally, as shown in Fig. 3d, CuN_3/NC/T-ZrO_2 has a lower Tafel slope, which indicates that electrons are transferred from the surface of CuN_3/NC/T-ZrO_2 to CO_2 molecules more easily for further reduction.[14] In contrast, the significantly reduced Tafel slope for the singly dispersed CuN_3 supported by T-ZrO_2 indicates that the kinetics of electron transfer is greatly enhanced. Moreover, to evaluate the electrochemically active surface area of the three catalysts, the values of the electrochemical double-layer capacitance (C_{dl}) were obtained using cyclic voltammetry (Fig. 3e). The C_{dl} values suggest that CuN_3/NC/T-ZrO_2 (27 mF cm^{-2}) possesses more active sites than CuN_3/NC/M-ZrO_2 (6 mF cm^{-2}), increasing the reaction speed of the electrocatalytic process. CuN_3/NC exhibits lower selectivity, which may be attributed to the lower CO_2 uptake for subsequent reduction, which is further proof of the essentialness of the T-ZrO_2 substrate during the EC-CO_2RR to CO. More importantly, CuN_3/NC/T-ZrO_2 exhibits excellent stability for the EC-CO_2RR, retaining approximately 95% of the initial

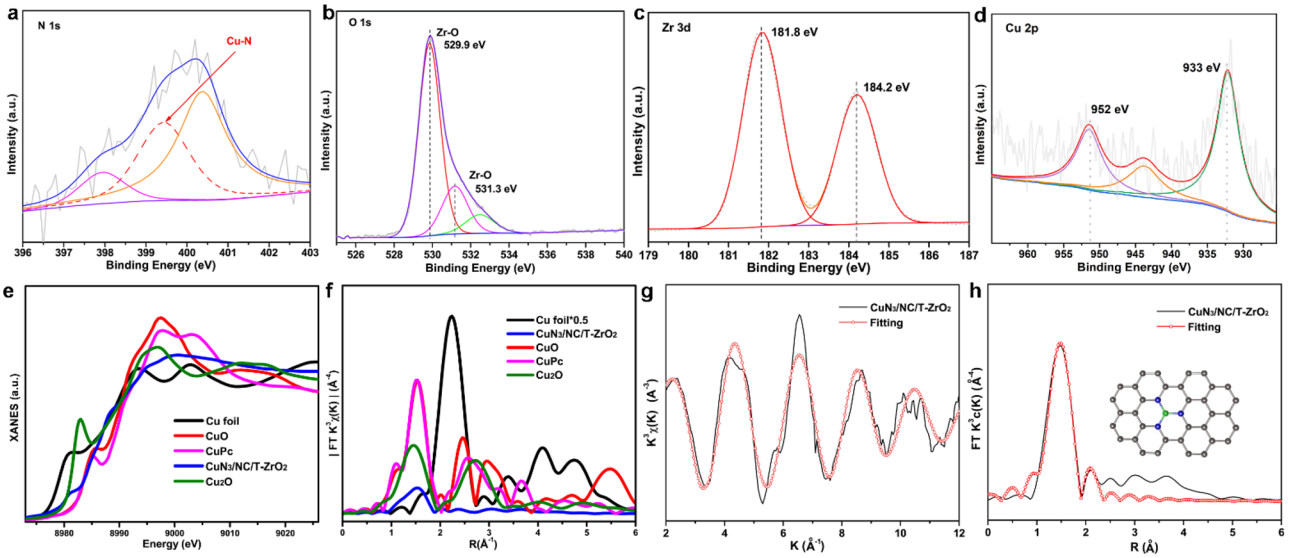

Fig. 2 (a–d) XPS spectra of CuN_3/NC/T-ZrO_2: N 2p, O 1s, Zr 3d, and Cu 2p, respectively. (e) Cu K-edge data of Cu foil, CuO, CuPc, Cu_2O, and CuN_3/NC/T-ZrO_2. (f) Fourier transform (FT) k^3-weighted EXAFS profiles at the Cu *k*-edge. (g) Fitting curves. (h) EXAFS R space fitting curves of CuN_3/NC/T-ZrO_2.

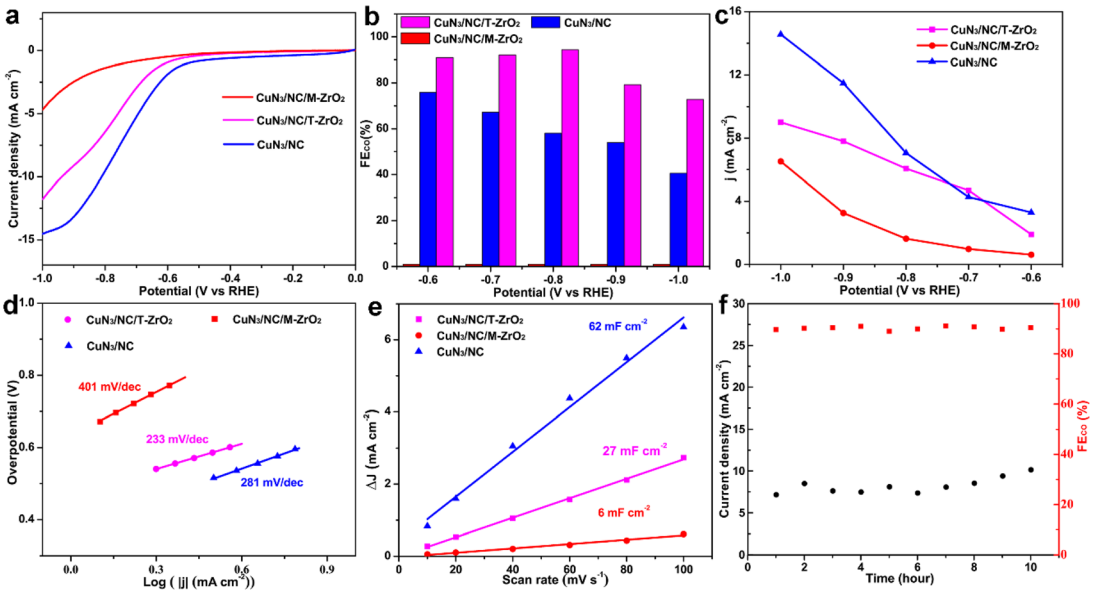

Fig. 3 Electrochemical catalytic performance of the catalysts in CO_2-saturated 0.5 M $KHCO_3$. (a) LSVs of CuN_3/NC/T-ZrO_2, CuN_3/NC/M-ZrO_2, CuN_3/NC. (b) Dependence of FE_{CO} for the catalysts. (c) Current densities at different potentials. (d) Tafel slopes of the catalysts. (e) Capacitances of the electrodes calculated from linear regression of the double-layer current as a function of scan rate. (f) Long-term stability performed at –1.0 *vs.* RHE.

faradaic efficiency for the CO product after 10 hours of continuous electrolysis. This result indicates that as a substrate, zirconia can support the active site well owing to its outstanding mechanical performance (Fig. 3f).

To further evaluate the effects of CuN_3/NC/T-ZrO_2 and CuN_3/NC/M-ZrO_2 catalysts on the activity and selectivity of the CO_2RR and HER, we applied density functional theory (DFT) to calculate the free energy and binding energy at each reaction intermediate step of the CO_2RR and HER. The most stable surfaces—the (101) face of tetragonal ZrO_2 (T-ZrO_2(101)) and (−111) of monoclinic ZrO_2 (M-ZrO_2(−111))—were employed to calculate the mechanism of the catalytic reaction (Fig. S9†).[15] Fig. 4a and b show the CO_2RR to CO reaction processes on CuN_3/NC/T-ZrO_2 and CuN_3/NC/M-ZrO_2, in which the protonation of CO_2 to form *COOH

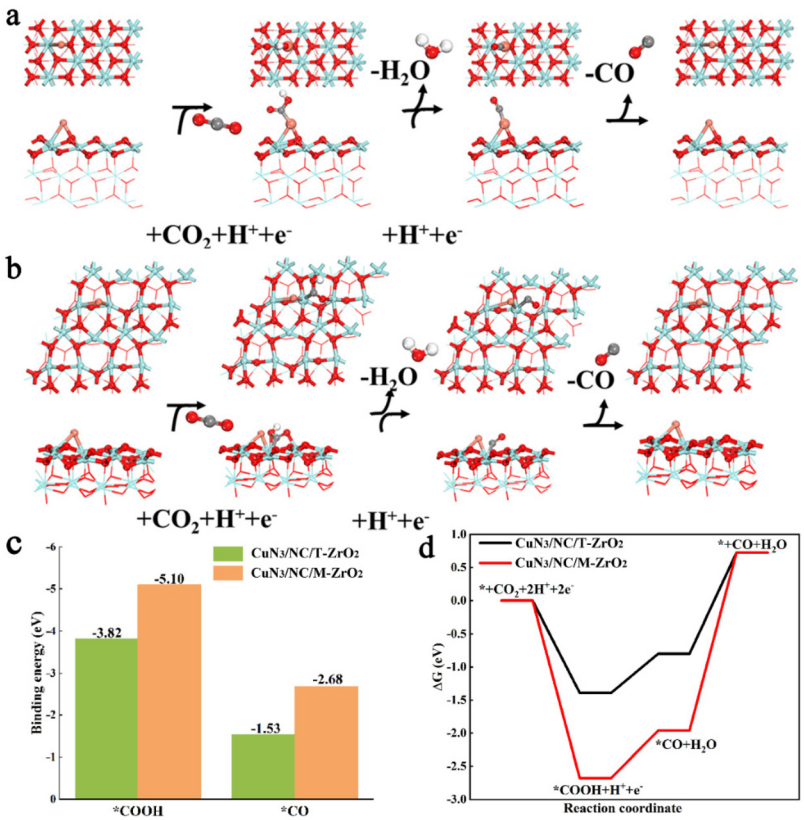

Fig. 4 (a) CO_2RR processes on CuN_3/NC/T-ZrO_2(101) and (b) CuN_3/NC/M-ZrO_2(−111). (c) Calculated binding energies (in eV) on CuN_3/NC/T-ZrO_2(101) and CuN_3/NC/M-ZrO_2(−111). (d) Calculated free energy diagrams of the CO_2RR on CuN_3/NC/T-ZrO_2(101) and CuN_3/NC/M-ZrO_2(−111).

could be identified as a potential limiting step.[16] Comparing Fig. 4a and b, the adsorption sites of the CO_2RR intermediates were different in various phases. The reaction intermediates *COOH and *CO were bound at the Cu site for CuN_3/NC/T-ZrO_2, while the reaction intermediates were bound at the Zr site for CuN_3/NC/M-ZrO_2. Noticeably, the binding energies of the intermediates are significantly stronger on CuN_3/NC/M-ZrO_2 than on CuN_3/NC/T-ZrO_2 (Fig. 4c). Although the relatively strong *COOH adsorption on the catalytic sites should improve the electrocatalytic activity, the strong binding of *CO on CuN_3/NC/M-ZrO_2 (BE = −2.68 eV) makes its desorption difficult. Furthermore, DFT calculations demonstrated that the energy barriers of CuN_3/NC/M-ZrO_2 are higher than those of CuN_3/NC/T-ZrO_2, suggesting poor activity of CuN_3/NC/M-ZrO_2 for the CO_2RR. Thus, CuN_3/NC/T-ZrO_2 exhibits the best selectivity for the CO_2RR.

The free energy of *H has been identified as a descriptor of the HER,[17] a competing reaction in the CO_2RR. Fig. 4d and 5 show that the free energy of *H on CuN_3/NC/M-ZrO_2 is below the free energy of *COOH, suggesting that the HER should be more favorable on CuN_3/NC/M-ZrO_2. Additionally, CuN_3/NC/T-ZrO_2 is expected to possess excellent CO selectivity owing to the weaker binding of *H compared to that of COOH*. The DFT results further demonstrate that CuN_3/NC/T-ZrO_2 favors CO formation while CuN_3/NC/M-ZrO_2 is active for H_2 evolution, which is consistent with our previously described experimental results.

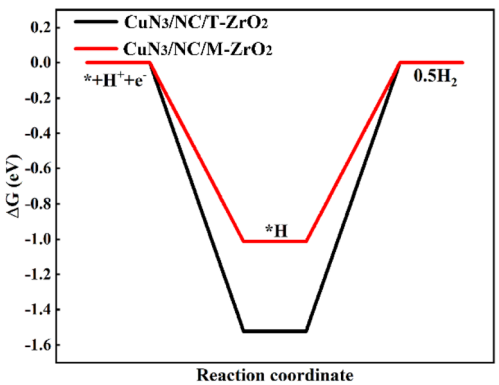

Fig. 5 DFT-calculated free energy diagrams of the HER on CuN_3/NC/T-ZrO_2(101) and CuN_3/NC/M-ZrO_2(−111) at a potential (U) = 0 V.

Conclusions

Herein, three EC-CO_2RR catalysts with singly dispersed Cu–N sites supported by ZrO_2 with different phases to tune the catalytic environment and enhance the selectivity for CO_2 conversion to CO have been designed and synthesized. The tetragonal phase of zirconia with acidic uncoordinated Zr^{4+} sites enhances C═O reduction, and N-doped carbon enhances the electrical conductivity of the catalysts. Together, the properties

of the catalysts afford the excellent ability of CO_2 to CO conversion of CuN_3/NC/T-ZrO_2. Systematic studies of CuN_3/NC/T-ZrO_2, CuN_3/NC/M-ZrO_2, and CuN_3/NC *via* experimentation and DFT calculation reveal that the acidic catalytic centre of the substrate plays a crucial factor in the generation of CO owing to its ability to concentrate CO_2 and prevent the HER. This work not only provides an in-depth understanding of the influence of the substrate during the electrocatalytic process but also provides a fundamental strategy to design promising catalysts for CO_2 to CO conversion with high selectivity and durability.

Conflicts of interest

There are no conflicts to declare.

Acknowledgements

This work was funded by the NSFC (Grant No. 21401004), Natural Science Foundation of Anhui Province (Grant No. 1508085QB36, 1908085QB58, 2008085MB52), and Open Foundation of Anhui Laboratory of Molecule-based Materials (fzj19005).

References

1 (*a*) J. E. Kay, Early climate models successfully predicted global warming, *Nature*, 2020, **578**, 45–46; (*b*) C. A. Logan, J. P. Dunne, J. S. Ryan, M. L. Baskett and S. D. Donner, Quantifying global potential for coral evolutionary response to climate change, *Nat. Clim. Change*, 2021, **11**, 537–542; (*c*) L. A. Parsons, D. Shindell, M. Tigchelaar, Y. Q. Zhang and J. T. Spector, Increased labor losses and decreased adaptation potential in a warmer world, *Nat. Commun.*, 2021, **12**, 7286; (*d*) M. Klower, M. R. Allen, D. S. Lee, S. R. Proud, L. Gallagher and A. Skowron, Quantifying aviation's contribution to global warming, *Environ. Res. Lett.*, 2021, **16**, 104027.

2 (*a*) I. Merino-Garcia, J. Albo, J. Solla-Gullón, V. Montiel and A. Irabien, Cu oxide/ZnO-based surfaces for a selective ethylene production from gasphase CO_2 electroconversion, *J. CO_2 Util.*, 2019, **31**, 135–142; (*b*) M. Loipersberger, D. G. A. Cabral, D. B. K. Chu and M. Head-Gordon, Mechanistic Insights into Co and Fe Quaterpyridine-Based CO_2 Reduction Catalysts: Metal-Ligand Orbital Interaction as the Key Driving Force for Distinct Pathways, *J. Am. Chem. Soc.*, 2021, **143**, 744–763; (*c*) K. Kosugi, M. Kondo and S. Masaoka, Quick and Easy Method to Dramatically Improve the Electrochemical CO_2 Reduction Activity of an Iron Porphyrin Complex, *Angew. Chem., Int. Ed.*, 2021, **60**, 22070–22074.

3 (*a*) Y. T. Liu, D. H. Deng and X. H. Bao, Catalysis for Selected C1 Chemistry, *Chem*, 2020, **6**, 2497–2514; (*b*) Y. J. Zhao, L. L. Zheng, D. Jiang, W. Xia, X. T. Xu, Y. Yamauchi, J. P. Ge and J. Tang, Nanoengineering Metal-Organic Framework-Based Materials for Use in Electrochemical CO_2 Reduction Reactions, *Small*, 2021, **17**, 2006590; (*c*) J. B. Jakobsen, M. H. Ronne, K. Daasbjerg and T. Skrydstrup, Are Amines the Holy Grail for Facilitating CO_2 Reduction, *Angew. Chem., Int. Ed.*, 2021, **60**, 9174–9179.

4 (*a*) S. R. Foit, I. C. Vinke, L. G. J. de Haart and R. A. Eichel, Power-to-Syngas: An Enabling Technology for the Transition of the Energy System, *Angew. Chem., Int. Ed.*, 2017, **56**, 5402–5411; (*b*) Q. He, D. B. Liu, J. H. Lee, Y. M. Liu, Z. H. Xie, S. Hwang, S. Kattel, L. Song and J. G. G. Chen, Electrochemical Conversion of CO_2 to Syngas with Controllable CO/H_2 Ratios over Co and Ni Single-Atom Catalysts, *Angew. Chem., Int. Ed.*, 2020, **59**, 3033–3037; (*c*) M. Zhang, Z. Hu, L. Gu, Q. H. Zhang, L. H. Zhang, Q. Song, W. Zhou and S. Hu, Electrochemical conversion of CO_2 to syngas with a wide range of CO/H_2 ratio over Ni/Fe binary single-atom catalysts, *Nano Res.*, 2020, **13**, 3206–3211.

5 (*a*) S. Z. Xu and E. A. Carter, Theoretical Insights into Heterogeneous (Photo)electrochemical CO_2 Reduction, *Chem. Rev.*, 2019, **119**, 6631–6669; (*b*) J. Y. Chen and L. Wang, Effects of the Catalyst Dynamic Changes and Influence of the Reaction Environment on the Performance of Electrochemical CO_2 Reduction, *Adv. Mater.*, 2021, 2103900; (*c*) S. Y. Liang, L. Huang, Y. S. Gao, Q. Wang and B. Liu, Electrochemical Reduction of CO2 to CO over Transition Metal/N-Doped Carbon Catalysts: The Active Sites and Reaction Mechanism, *Adv. Sci.*, 2021, **8**, 2102886.

6 (*a*) Y. L. Jia, Z. Q. Xue, J. Yang, Q. L. Liu, J. H. Xian, Y. C. Zhong, Y. M. Sun, X. X. Zhang, Q. H. Liu, D. X. Yao and G. Q. Li, Tailoring the Electronic Structure of an Atomically Dispersed Zinc Electrocatalyst: Coordination Environment Regulation for High Selectivity Oxygen Reduction, *Angew. Chem., Int. Ed.*, 2022, **61**, e202110838; (*b*) R. R. Yun, T. H. Li, B. B. Zhang, L. He, S. J. Liu, C. Yu, Z. Chen and S. Z. Luo, Amino induced high-loading atomically dispersed Co sites on N-doped hollow carbon for efficient CO_2 transformation, *Chem. Commun.*, 2022, **58**, 6602–6605; (*c*) L. L. Wan, X. L. Zhang, J. S. Cheng, R. Chen, L. X. Wu, J. W. Shi and J. S. Luo, Bimetallic Cu-Zn Catalysts for Electrochemical CO2 Reduction: Phase-Separated versus Core-Shell Distribution, *ACS Catal.*, 2022, **12**, 2741–2748.

7 (*a*) J. Albo, D. Vallejo, G. Beobide, O. Castillo, P. CastaÇo and A. Irabien, Copper-Based Metal–Organic Porous Materials for CO2 Electrocatalytic Reduction to Alcohols, *ChemSusChem*, 2017, **10**, 1100–1109; (*b*) L. Y. Ouyang, V. Noel, A. Courty, J. M. Campagne, A. Ouali and E. Vrancken, Copper Nanoparticles with a Tunable Size: Implications for Plasmonic Catalysis, *ACS Appl. Nano Mater.*, 2022, **5**(2), 2839–2847.

8 (*a*) M. R. Han, Y. N. Zhou, X. Zhou and W. Chu, Tunable Reactivity of MNi12 (M = Fe, Co, Cu, Zn) Nanoparticles Supported on Graphitic Carbon Nitride in Methanation,

Acta Phys. – Chim. Sin., 2019, **35**, 850–857; (*b*) A. Halder, C. Lenardi, J. Timoshenko, A. Mravak, B. Yang, L. K. Kolipaka, C. Piazzoni, S. Seifert, V. Bonacic-Koutecky, A. I. Frenkel, P. Milani and S. Vajda, CO_2 Methanation on Cu-Cluster Decorated Zirconia Supports with Different Morphology: A Combined Experimental In Situ GIXANES/GISAXS, Ex Situ XPS and Theoretical DFT Study, *ACS Catal.*, 2021, **11**, 6210–6224.

9 (*a*) G. P. Gao, S. Bottle and A. J. Du, Understanding the activity and selectivity of single atom catalysts for hydrogen and oxygen evolution via ab initial study, *Catal. Sci. Technol.*, 2018, **8**, 996–1001; (*b*) Y. F. Wang, M. Jin, X. Zhang, C. J. Zhao, H. J. Wang, S. H. Li and Z. Y. Liu, Direct Conversion of Biomass into Compact Air Electrode with Atomically Dispersed Oxygen and Nitrogen Coordinated Copper Species for Flexible Zinc-Air Batteries, *ACS Appl. Energy Mater.*, 2019, **2**, 8659–8666.

10 (*a*) J. F. de Souza, M. S. Gularte, R. F. N. Quadrado, A. F. P. Biajoli and A. R. Fajardo, Copper species supported in polysaccharide-based materials: from preparation to application in catalysis, *Catal. Rev.*, 2021, 1904543; (*b*) I. Merino-Garciaa, J. Alboa, P. Krzywdab, G. Mulb and A. Irabien, Bimetallic Cu-based hollow fibre electrodes for CO2 electroreduction, *Catal. Today*, 2020, **346**, 34–39.

11 Y. Hisai, Q. B. Ma, T. Qureishy, T. Watanabe, T. Higo, T. Norby and Y. Sekine, Enhanced activity of catalysts on substrates with surface protonic current in an electrical field - a review, *Chem. Commun.*, 2021, **57**, 5737–5749.

12 (*a*) M. Yang, J. F. Yu, X. Tong, X. T. Sun, H. Y. Xu and J. Sun, Flame-made Cu/ZrO2 catalysts with metastable phase and strengthened interactions for CO2 hydrogenation to methanol, *Chem. Commun.*, 2021, **57**, 7509–7512; (*b*) J. Lu, Y. Zhang, S. Wang and Z. Li, Preparation of highly dispersed CuO-ZnO-ZrO_2 catalysts and their improved catalytic performance for hydrogenation of CO_2, *Can. J. Chem.*, 2022, **100**, 387–395.

13 (*a*) T. Ghodselahi, M. A. Vesaghi, A. Shafiekhani, A. Baghizadeh and M. Lameii, XPS study of the Cu@Cu_2O core-shell nanoparticles, *Appl. Surf. Sci.*, 2008, **255**, 2730–2734; (*b*) G. U. Kulkarni and C. N. R. Rao, EXAFS and XPS investigations of Cu/ZnO catalysts and their interaction with CO and methanol, *Top. Catal.*, 2003, **22**, 183–189.

14 R. R. Yun, F. Y. Zhan, X. J. Wang, B. B. Zhang, T. Sheng, Z. F. Xin, J. J. Mao, S. J. Liu and B. S. Zheng, Design of Binary Cu-Fe Sites Coordinated with Nitrogen Dispersed in the Porous Carbon for Synergistic CO2 Electroreduction, *Small*, 2021, **17**, 2006951.

15 A. Christensen and E. A. Carter, First-Principles Study of the Surfaces of Zirconia, *Matter Mater. Phys.*, 1998, **58**, 8050–8064.

16 J. T. Feaster, C. Shi, E. R. Cave, T. Hatsukade, D. N. Abram, K. P. Kuhl, C. Hahn, J. K. Nørskov and T. F. Jaramillo, Understanding Selectivity for the Electrochemical Reduction of Carbon Dioxide to Formic Acid and Carbon Monoxide on Metal Electrodes, *ACS Catal.*, 2017, **7**, 4822–4827.

17 J. K. Nørskov, T. Bligaard, A. Logadottir, J. R. Kitchin, J. G. Chen, S. Pandelov and U. Stimming, Trends in the Exchange Current for Hydrogen Evolution, *J. Electrochem. Soc.*, 2005, **152**, J23–J26.